

Supporting Information

Every Atom Counts: Elucidating the Fundamental Impact of Structural Change in Conjugated Polymers for Organic Photovoltaics

Chi Kin Lo,[†] Bhoj R. Gautam,^{‡,*} Philipp Selzer,[§] Zilong Zheng,[†] Stefan D. Oosterhout,^{||} Iordania Constantinou,^{Δ,#} Robert Knitsch,[§] Rylan M.W. Wolfe,[†] Xueping Yi,^Δ Jean-Luc Brédas,[†] Franky So,^Δ Michael F. Toney,^{||} Veaceslav Coropceanu,[†] Michael Ryan Hansen,[§] Kenan Gundogdu,[‡] John R. Reynolds^{†,*}

[†] School of Chemistry and Biochemistry, Center for Organic Photonics and Electronics, Georgia Tech Polymer Network, Georgia Institute of Technology, Atlanta, GA 30332, USA

[‡] Department of Physics, North Carolina State University, Raleigh, NC 27695, USA

^{*} Department of Chemistry and Physics, Fayetteville State University, Fayetteville, NC 28301, USA

[§] Institute of Physical Chemistry, Westfälische Wilhelms-Universität Münster, Corrensstr. 28/30, D-48149 Münster, Germany

^{||} SLAC National Accelerator Laboratory, Stanford University, Menlo Park, CA, 94025, USA

^Δ Department of Materials Science and Engineering, North Carolina State University, Raleigh, NC 27695, USA

*Corresponding Author's Email: reynolds@chemistry.gatech.edu

#Current address: Iordania Constantinou - Zentrum für Molekulare Biologie (ZMBH), Universität Heidelberg, Heidelberg, Germany, 69120

Contents

Experimental Details	3
Materials and Methods	3
Synthesis of Monomers	4
Synthesis of Polymers	5
ICP-MS and microwave-assisted digestion of polymer matrix	6
Polymer Molecular Weight Estimation by Gel Permeation Chromatography	7
Literature Comparison	8
Computational Methodology	9
Electronic Properties	13
Steady-state Optical Absorption Properties	14
Solid State NMR Measurements and Characterizations	15
OPV Device Fabrication and Characterization	17
Methods	17
X-Ray Diffraction Measurement with Thermal Annealing	18
Thermal Transition of Polymers	20
Topographical Characteristic of Polymer:PCBM Thin Films	21
Transient Absorption Properties	22
References	26

Experimental Details

Materials and Methods

PEDOT:PSS (Clevios™ P VP AI 4083) was purchased from Heraeus Deutschland GmbH & Co. KG. PC71BM was purchased from Nano-C. Solvents used in polymerizations and device fabrications were dried with 4 Å molecular sieves and degassed via at least four freeze, pump, thaw cycles. All reactions were carried out under an argon atmosphere. Silica (60 Å porosity, 40-64 μm particle size) was purchased from Sorbent Technologies, Inc for use in column chromatography. All other starting materials were purchased from commercial suppliers and used without further purifications. 2,6-dibromo-4,4-bis(2-ethylhexyl)-cyclopenta[2,1-b:3,4-b']dithiophene (dibromo-CPDT or dibromo-DTC) was purchased from Bepharma.

Elemental analyses were conducted by Atlantic Microlab, Inc. Absorption spectra were measured using a Varian Cary 5000 Scan UV-Vis-NIR spectrophotometer. HPLC purifications were carried out on a Shimadzu (SCL-10AVP) HPLC system with a (250 mm x 22 mm C18? reversed-phase column), a flow rate of 15 mL/min, and two (Shimadzu SPD-10AV and SPD-M10A) UV-Vis detectors operating at 330 nm and 350 nm. The molecular weight and dispersity of the polymers were determined by gel permeation chromatography (GPC) using a Tosoh Bioscience EcoSEC High Temperature GPC system HLC-8321GPC/HT with RI detector. Experiments were carried out with 1,2,4-trichlorobenzene as the eluent at a flow rate of 1 mL/min at 140 °C on two 7.8 mm × 30 cm, 13 μm TSK-Gel GMH_{HR}-H(S) HT2 columns in series (Tosoh Bioscience). The instrument was calibrated using polystyrene standards (4,930–1,214,000 g/mol) and the data were analysed using 8321GPC-WS Analysis software. Thermogravimetric analyses were carried out on a PerkinElmer Pyrus 1 TGA under a continuous flow of nitrogen with a heating rate of 10 °C/min. Differential scanning calorimetry results were performed using a TA Instruments Q200 DSC with a heating rate and a cooling rate of 10 °C/min in hermetically sealed aluminum pans. Electrochemistry was performed using an EG&G Princeton Applied Research model 273A potentiostat-galvanostat. Cyclic voltammograms (scan rate 50 mV/s) and differential pulse voltammograms (step size 2 mV, step time 50 ms, pulse amplitude 100 mV) were collected using 0.01 cm² Pt disc electrodes (polymer films were dropcast from 1 mg/mL chloroform solutions) in 0.5M TBAPF₆/acetonitrile, with a Ag/Ag⁺ reference electrode (0.01 M AgNO₃) and a Pt flag counter electrode. The reference electrode was calibrated against the ferrocene/ferrocenium couple which is taken to be -5.1 V vs. vacuum.¹ The atomic force microscopy (AFM) images were obtained with a Bruker Icon AFM microscope operating in tapping mode.

For molecular precursors, solution ¹H and ¹³C NMR spectra were collected using a Varian Mercury Vx 300 MHz spectrometer. The chemical shifts were recorded in units of ppm and referenced to the residual solvent peak of chloroform-d, ¹H: δ = 7.26 ppm, ¹³C: δ = 77.23 ppm. For polymer samples, solution ¹H NMR spectra were collected using Bruker Corporation DRX 500 MHz spectrometer. The chemical shifts were recorded in units of ppm and referenced to the residual solvent peaks of chlorobenzene-d₅, ¹H: δ = 6.96, 6.99, and 7.14 ppm.

Synthesis of Monomers

For proper naming of heterocycles, the reader is encouraged to read *The nomenclature of fused-ring arenes and heterocycles: a guide to an increasingly important dialect of organic chemistry* by Rasmussen.²

4,4-bis(2-ethylhexyl)-2,6-bis(trimethylstannyl)cyclopenta[2,1-*b*:3,4-*b'*]dithiophene was synthesized according to a modified literature procedure.³ To a 100 mL round bottom flask, 2,6-dibromo-4,4-bis(2-ethylhexyl)-cyclopenta[2,1-*b*:3,4-*b'*]dithiophene (1.69 g, 3 mmol) and THF (30 mL) were added. The mixture was cooled to -78 °C and *n*-BuLi (7.2 mL of 2.5 M in hexanes, 18 mmol) was added dropwise over 30 minutes. The mixture was allowed to warm to room temperature and stirred for 1 hour, then cooled back to -78 °C. Trimethyltin chloride (21 mL of 1.0 M in anhydrous THF, 21 mmol) was added to the reaction mixture dropwise over 30 minutes. The reaction was returned to room temperature and stirred overnight at room temperature. The mixture was quenched with water (30 mL) and extracted with hexanes (3 × 100 mL). The combined organic portions were washed with sodium bicarbonate solution (100 mL), water (2 × 100 mL), and brine (50 mL), before being dried over MgSO₄. After solvent was removed under reduced pressure, the crude yellow oil was purification by reversed phase HPLC (60:40 ACN:acetone) to afford a clear oil. (1.3 g, 1.8 mmol, 60%). ¹H NMR (300 Hz, CDCl₃, ppm): δ 6.99 (s, 2H), 1.83 (m, 4H), 1.32 (m, 2H), 0.91 (m, 16H), 0.78 (t, *J* = 6.9 Hz, 6H), 0.64 (t, *J* = 7.2 Hz, 6H), 0.37 (m, 18H).

4,4-bis(2-ethylhexyl)-2,6-bis(trimethylstannyl)silolo[3,2-*b*:4,5-*b'*]dithiophene (DTS) and **4,4-bis(2-ethylhexyl)-2,6-bis(trimethylstannyl)germolo[3,2-*b*:4,5-*b'*]dithiophene (DTG)** were synthesized according to published procedures.^{4,5} The crude yellow oils were purification by reversed phase HPLC (60:40 ACN:acetone).

5-Octylthieno[3,4-*c*]pyrrole-4,6-dione.^{6,7} To a 300 mL round bottom flask thiophene-3,4-dicarboxylic acid (6.0 g, 35 mmol) and acetic anhydride (150 mL) were added and stirred at 140 °C overnight. The solvent was removed under reduced pressure to afford thieno[3,4-*c*]furan-1,3-dione as brown crystals (5.2 g, 34 mmol, 97%) which were used in the next step without purification. To a 500 mL round bottom flask, 5.2 g of thieno[3,4-*c*]furan-1,3-dione, *n*-octylamine (7.0 g, 51 mmol, 1.5 equiv) and toluene (300 mL) were added. A condenser was attached to the flask, and the mixture was refluxed for 24 hours. After cooling to room temperature, the solvent was removed under reduced pressure. The air-sensitive brown oil was dissolved in thionyl chloride (200 mL) and the mixture was refluxed for 4 hours. The reaction was cooled to room temperature and quenched with MeOH (200 mL). Water (200 mL) was added to the crude mixture, which was extracted with DCM. The combined organics were washed with water (2 × 150 mL) then brine (100 mL), and dried over MgSO₄. After the solvent was removed under reduced pressure, the crude solid was purified by column chromatography using 1:1 hexanes:DCM. The brown solid was further purified by recrystallization in hexanes to afford white needles (3.4 g, 13 mmol, 37%). ¹H NMR (300 Hz, CDCl₃, ppm): δ: 7.80 (s, 2H), 3.60 (t, *J* = 7.2 Hz, 2H), 1.64 (m, 2H), 1.25 (m, 10H), 0.87 (t, *J* = 6.8 Hz, 3H).

1,3-Dibromo-5-octylthieno[3,4-*c*]pyrrole-4,6-dione.^{6,7} To a 100 mL round bottom flask, 5-octylthieno[3,4-*c*]pyrrole-4,6-dione (2.7 g, 10 mmol) was dissolved in a mixture of sulfuric acid (15 mL) and trifluoroacetic acid (50 mL) at room temperature. *N*-bromosuccinimide (5.4 g, 30 mmol) was added in three portions over 15 minutes and the reaction mixture was stirred at room temperature for 12 hours. The reaction was monitored by TLC for the disappearance of the starting material. After the reaction was completed, the mixture was poured into water (100 mL) and extracted with DCM (2 × 30 mL). The combined organics were washed with water (2 × 100 mL) then brine (100 mL), and dried over MgSO₄. After the solvent was removed under reduced pressure, the crude product was purified by column chromatography using 1:1 hexanes:DCM to afford white crystals (3.3 g, 79%). ¹H NMR (300 Hz, CDCl₃, ppm): δ: 3.59 (t, *J* = 7.2 Hz, 2H), 1.63 (m, 2H), 1.26 (m, 10H), 0.87 (t, *J* = 6.7 Hz, 3H).

Synthesis of Polymers

General Procedures of Stille Cross-Coupling Polymerizations for Poly(4,4-bis(2-ethylhexyl)cyclopenta[2,1-*b*:3,4-*b'*]dithiophen-2,6-diyl-*alt*-5-octylthieno[3,4-*c*]pyrrol-4,6-dione-1,3-diyl), P(DTC-TPD)

Poly(4,4-bis(2-ethylhexyl)silolo[3,2-*b*:4,5-*b'*]dithiophen-2,6-diyl-*alt*-5-octylthieno[3,4-*c*]pyrrol-4,6-dione-1,3-diyl), P(DTS-TPD)

Poly(4,4-bis(2-ethylhexyl)germolo[3,2-*b*:4,5-*b'*]dithiophen-2,6-diyl-*alt*-5-octylthieno[3,4-*c*]pyrrol-4,6-dione-1,3-diyl), P(DTG-TPD)

To a 25 mL Schlenk tube, 1,3-dibromo-5-octylthieno[3,4-*c*]pyrrole-4,6-dione (408 mg, 1 mmol) and a ditin-dithiophene monomer (1 mmol) were added and purged with argon for 3 pump-fill cycles. Pd₂(dba)₃ (14.9 mg, 1.5 mol% catalyst loading or 3 mol% Pd), and P(*o*-tol)₃ (13.1 mg, 4.5 mol%) were added to a vial in an argon-filled glovebox and sealed with a septum to prevent ambient exposure after removal from the glovebox. Toluene (5 mL) was added to the vial to dissolve the catalyst and ligand; a quick sonication was helpful to ensure full dissolution. To the Schlenk tube, toluene (5 mL) was added, followed by the catalyst and ligand *via* a syringe and needle. The reaction mixture was heated to 90 °C and stirred for 72 hours. After the polymerization, 2-(tributylstannyl)thiophene (0.1 mL, 0.3 mmol) was added and stirred for 14 hours at 90 °C, followed by the addition of 2-bromothiophene (0.1 mL, 1 mmol). The mixture was stirred for an additional 10 hours. After cooling to 60 °C, a spatula-tip amount of diethyldithiocarbamic acid diethylammonium salt (CAS# 2391-78-8) was added and stirred for 10 hours to scavenge the palladium catalyst. A portion of toluene (10 mL) was added and the mixture was precipitated into methanol and collected on a 0.45 μm nylon filter. The crude polymer underwent soxhlet extractions with following order of solvents: methanol, acetone, hexanes, dichloromethane, and chloroform until each wash was colorless. The chloroform fraction was concentrated to a volume in which the entire sample was still soluble in room temperature chloroform (approximately 150 mL). The mixture was passed through a 4" plug of

1:1:1 (by volume) mixture of silica, basic alumina, and celite. Additional chloroform was used as the eluent until all polymer had passed through the plug. The polymer was concentrated to a dry solid. The polymer was dissolved in a minimal amount of chloroform and filtered through a 0.45 μm nylon filter directly into a large excess of acetone. The precipitated polymer was allowed to stir for 30 min before being collected on a 0.45 μm nylon filter. The polymer was dried under vacuum for 24 hours and obtained as a dark blue solid.

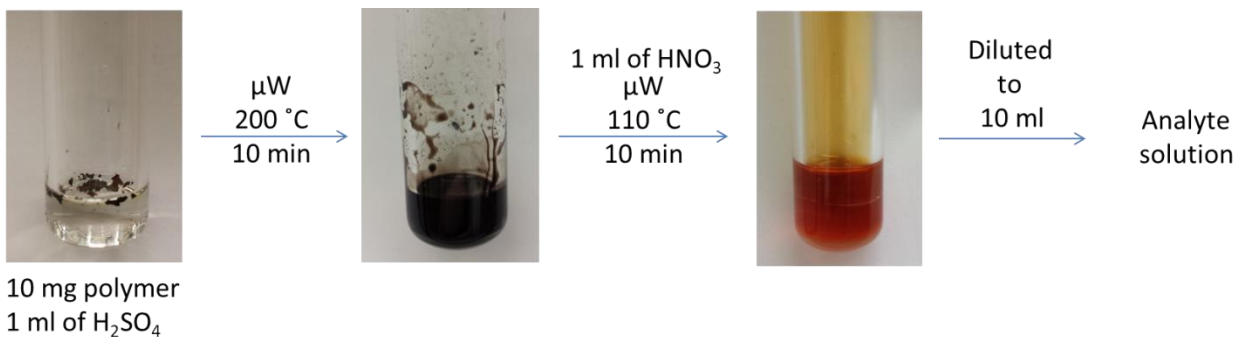
P(DTC-TPD). 375 mg (59%). GPC (1,3,4-trichlorobenzene at 140 °C vs polystyrene standards, RI): $M_n = 26.4$ kg/mol, $D_M = 1.4$. Anal. Calcd for $\text{C}_{39}\text{H}_{53}\text{NO}_2\text{S}_3$ (%): C, 70.54; H, 8.04; N, 2.11; S, 14.49. Found (%): C, 70.54; H, 8.14; N, 2.16; S, 14.57.

P(DTS-TPD). 423 mg (67%). GPC (1,3,4-trichlorobenzene at 140 °C vs polystyrene standards, RI): $M_n = 24.5$ kg/mol, $D_M = 1.7$. Anal. Calcd for $\text{C}_{38}\text{H}_{53}\text{NO}_2\text{S}_3\text{Si}$ (%): C, 67.11; H, 7.85; N, 2.06; S, 14.1. Found (%): C, 67.25; H, 7.85; N, 2.10; S, 14.47.

P(DTG-TPD). 483 mg (73%). GPC (1,3,4-trichlorobenzene at 140 °C vs polystyrene standards, RI): $M_n = 20.8$ kg/mol, $D_M = 1.7$. Anal. Calcd for $\text{C}_{38}\text{H}_{53}\text{NO}_2\text{S}_3\text{Ge}$ (%): C, 62.98; H, 7.37; N, 1.93; S, 13.27. Found (%): C, 63.06; H, 7.20; N, 2.03; S, 13.42.

ICP-MS and microwave-assisted digestion of polymer matrix

Trace element analysis on palladium, tin, and phosphorus residual contents was performed at in the Department of Geological Sciences at the University of Florida using ThermoFinnigan Element2 HR-ICP-MS. To a 10 mL microwave vial, approximately 10 mg of precisely massed polymer matrix and 1 mL of conc. H_2SO_4 were added. The vial was heated to 200 °C for 10 minutes in a microwave reactor (< 300 psi). Subsequently, 1 mL of conc. HNO_3 was added to the microwave vial and heated to 110 °C in a microwave reactor for 10 minutes to fully digest the polymer matrix. A control containing a mixture of the mineral acids was used as a reference. Note that heating with H_2SO_4 and HNO_3 (1:1 ratio mixture) in an oil bath was unsuccessful in fully digesting the polymer matrix. Aqua regia was also used but the outcome was similarly dissatisfying.



Polymer Molecular Weight Estimation by Gel Permeation Chromatography

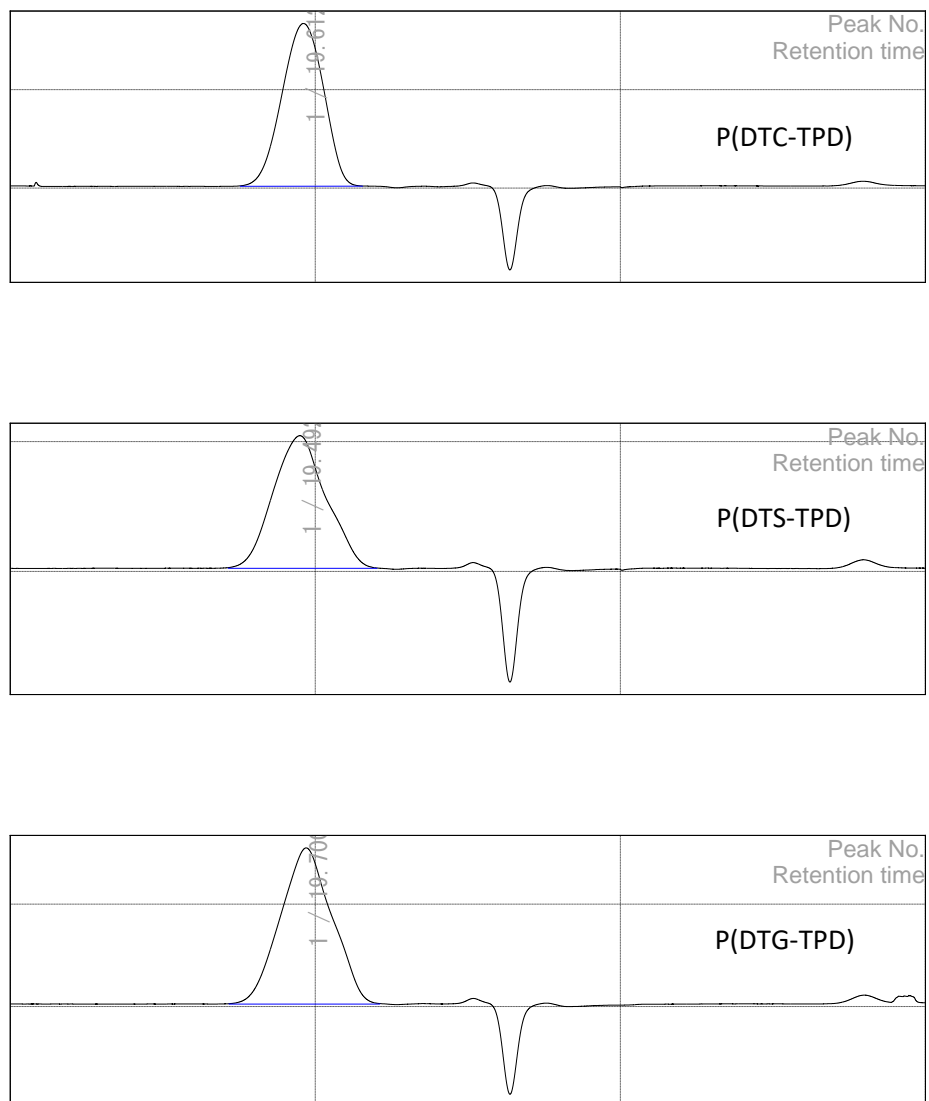


Figure S1. Gel permeation chromatograms of the polymers. The negative peaks following the sample peaks are resulting from air bubble entering the column during injections. Note all chromatograms show mono-modal peaks.

Literature Comparison

Table S1. Published properties of polymers with the same backbones as in this article.

Polymer	M _n (kg/mol)	D _M	Catalyst	Ligand	IP (eV)	EA (eV)	Film λ ^{onset} (nm)	Polymer to PCBM Ratio ¹	Additive	Solvent	Device ²	V _{oc} (V)	J _{sc} (mA/cm ²)	FF	PCE	Ref
DTC	16.0	1.26	Pd(PPh ₃) ₄	-	-5.73	-3.55	741	1:2	None	o-DCB	C	0.80	10.0	47.0%	3.7%	⁸
	16.0	1.26	Pd(PPh ₃) ₄	-	-5.73	-3.55	741	1:2	2% CN	o-DCB	C	0.80	9.4	45.0%	3.5%	⁸
	17.0	1.25	Pd ₂ (dba) ₃	P(o-tol) ₃	-5.67	-3.95	740	1:1	None	o-DCB	C	0.86	8.5	43.0%	3.1%	⁹
	17.0	1.25	Pd ₂ (dba) ₃	P(o-tol) ₃	-5.67	-3.95	740	1:2	None	o-DCB	C	0.86	6.9	48.0%	2.9%	⁹
DTS	13.6	1.43	Pd(PPh ₃) ₄	-	-5.74	-3.47	734	1:2	None	o-DCB	C	0.91	2.3	56.0%	1.2%	⁸
	13.6	1.43	Pd(PPh ₃) ₄	-	-5.74	-3.47	734	1:2	2% CN	o-DCB	C	0.85	6.6	37.0%	2.1%	⁸
	24.2	2.40	Pd(PPh ₃) ₄	-			740	1:1.5	2.5% DIO	o-DCB	C	0.91	11.1	50.0%	5.0%	¹⁰
	17.0	2.11	Pd(PPh ₃) ₄	-	-	-	740	1:2	30 mg/mL 1,5-DMN	TMB	I	0.90	13.5	66.8%	8.1%	¹¹
	17.0	2.11	Pd(PPh ₃) ₄	-	-	-	740	1:2	3% DIO	CB	I	0.91	12.3	65.4%	7.3%	¹¹
	-	-	-	-	-	-	-	1:2	3% DIO	o-DCB	C	0.90	11.0	63.0%	6.2%	¹²
	-	-	-	-	-	-	-	1:1.5	2% MeN + 3% DIO	Xylene	C	0.89	11.7	59.0%	6.2%	¹²
	29.0	1.80	Pd ₂ (dba) ₃	P(o-tol) ₃	-5.82	-4.09	717	1:2	3% DIO	CB	I	0.89	11.9	64.9%	6.8%	¹³
	31.0	1.58	-	-	-	-	717	1:2	3% DIO	CB	C	0.91	12.1	70.0%	7.5%	¹³
	42.5	1.54	Pd ₂ (dba) ₃		-5.65	-3.50	717	1:1.5	5% DIO	CB	I	0.89	11.5	65.0%	6.6%	⁴
DTG	16.3	1.90	Pd(PPh ₃) ₄	-	-5.76	-4.03	742	1:2	3% DIO	CB	C	0.80	9.7	53.0%	4.1%	¹⁴
	-	-	Pd ₂ (dba) ₃	P(o-tol) ₃	-	-	-	1:1.5	5% DIO	CB	C	0.86	15.9	63.0%	8.5%	¹⁵
	47.5	1.73	Pd ₂ (dba) ₃	P(o-tol) ₃	-5.60	-3.50	734	1:1.5	5% DIO	CB	I	0.86	14.0	67.3%	8.5%	¹⁶
	47.5	1.73	Pd ₂ (dba) ₃	P(o-tol) ₃	-5.60	-3.50	734	1:1.5	5% DIO	CB	I	0.85	12.6	68.0%	7.3%	⁴

¹ All devices use PC₇₁BM as the acceptor.

² Device architecture – C = Conventional; I = Inverted.

Computational Methodology

The ground-state geometries of all studied systems were optimized using density functional theory (DFT) calculations at the B3LYP/6-31G(d) level. Electronic-structure calculations were then performed by means of the optimally tuned long-range corrected functional ω B97XD.¹⁷ The optimally tuned values of the range-separated parameters (ω) were obtained by minimizing the function $J(\omega)$ ¹⁸ and taking into account the effect of the dielectric medium within the polarizable continuum model (PCM)¹⁹ assuming a dielectric constant $\epsilon=3$:

$$J(\omega) = [\epsilon_{HOMO}(\omega) - IP(\omega)]^2 + [\epsilon_{LUMO}(\omega) - EA(\omega)]^2$$

Here, ϵ_{HOMO} and ϵ_{LUMO} are the energies of highest occupied and lowest unoccupied molecular orbitals (HOMO and LUMO); IP and EA denote the vertical first ionization potential and electron affinity of the system. The derived optimally tuned values of ω are given in Table S2.

The excited-state energies were obtained by means of time-dependent DFT calculations (TD-DFT) based on the Tamm-Dancoff approximation (TDA).²⁰ The excited states of the polymers were modeled using oligomers with up to five DTX-TPD repeat units. The calculated energies of the frontier orbitals of the DTC-TPD oligomers (Figure S2 and Tables S2-S3) with an increasing number of units from one to five, shows that five repeat units are sufficient for the convergence of the frontier orbital energies. For instance, the difference between E_{HOMO} (E_{LUMO}) of (DTC-TPD)_{n=4} and (DTC-TPD)_{n=5} is less than 0.02 (0.05) eV.

The relaxation energies of the first excited state were computed in two ways: (a) they were computed directly from the adiabatic potential-energy surfaces of the ground and S_1 states; and (b) they were obtained on the basis of a normal-mode analysis, which provides as well the partition of the total relaxation energy into the contributions from each vibrational mode (see Figure S4).²¹ These calculations were performed at the B3LYP/6-31G(d) level using monomer units for polymers. The same level of calculations was used to evaluate the torsional potentials of the polymers (see Figure S3).

The geometry optimization were performed by means Gaussian09²² package while the calculations of the torsional potentials and excited-state energies were performed with Q-chem 4 package.^{23,24}

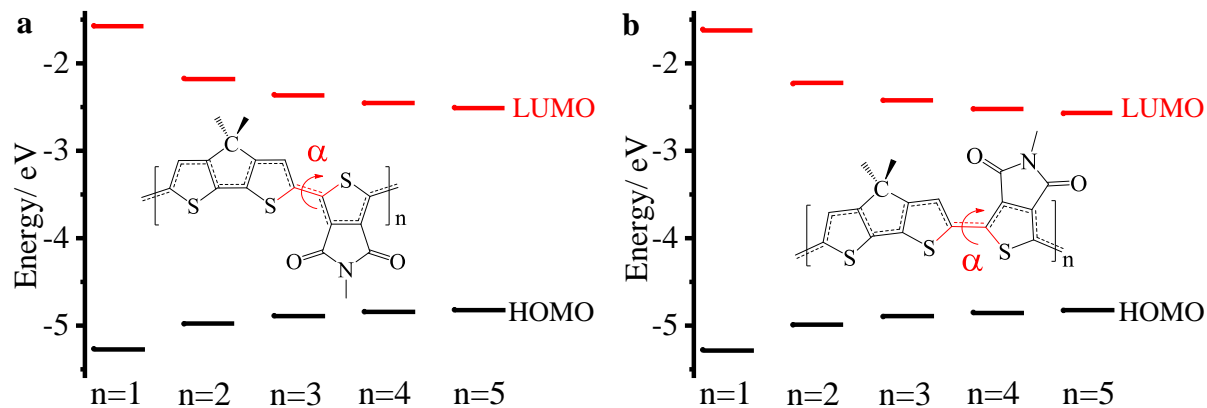


Figure S2. The estimated energies of the frontier molecular orbitals of the $(\text{DTC-TPD})_n$ oligomers: (a) anti-conformation, and (b) syn-conformation. The calculations are performed at the tuned- $\omega\text{B97XD/PCM}$ level with the 6-31G(d) basis set.

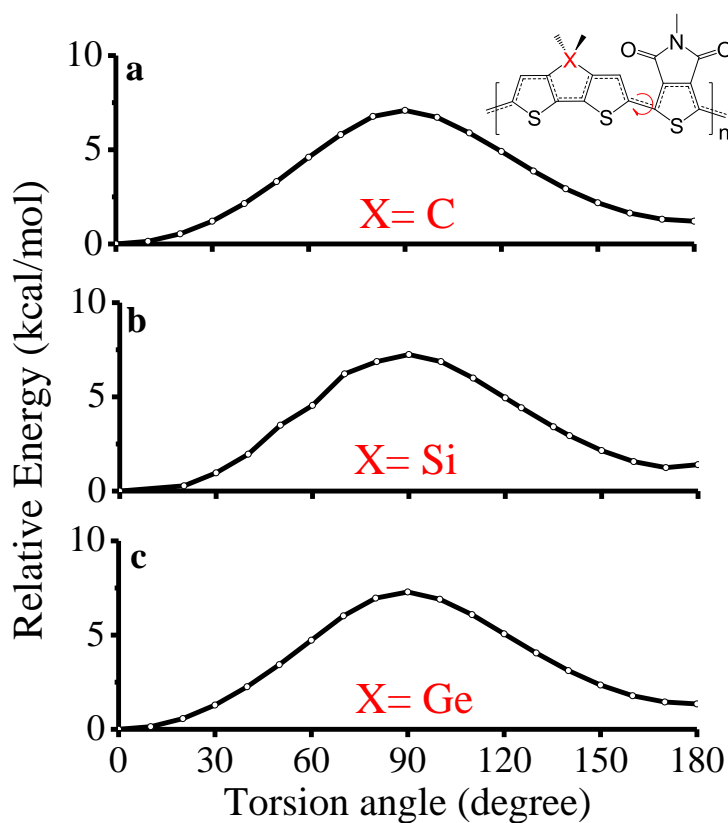


Figure S3. Torsional potentials of (a) P(DTC-TPD), (b) P(DTS-TPD), and (c) P(DTG-TPD). Rotation occurs around the inter-ring C–C bond between the DTC (DTS, DTG) and TPD. The calculations were performed at the B3LYP/6-31G(d) level.

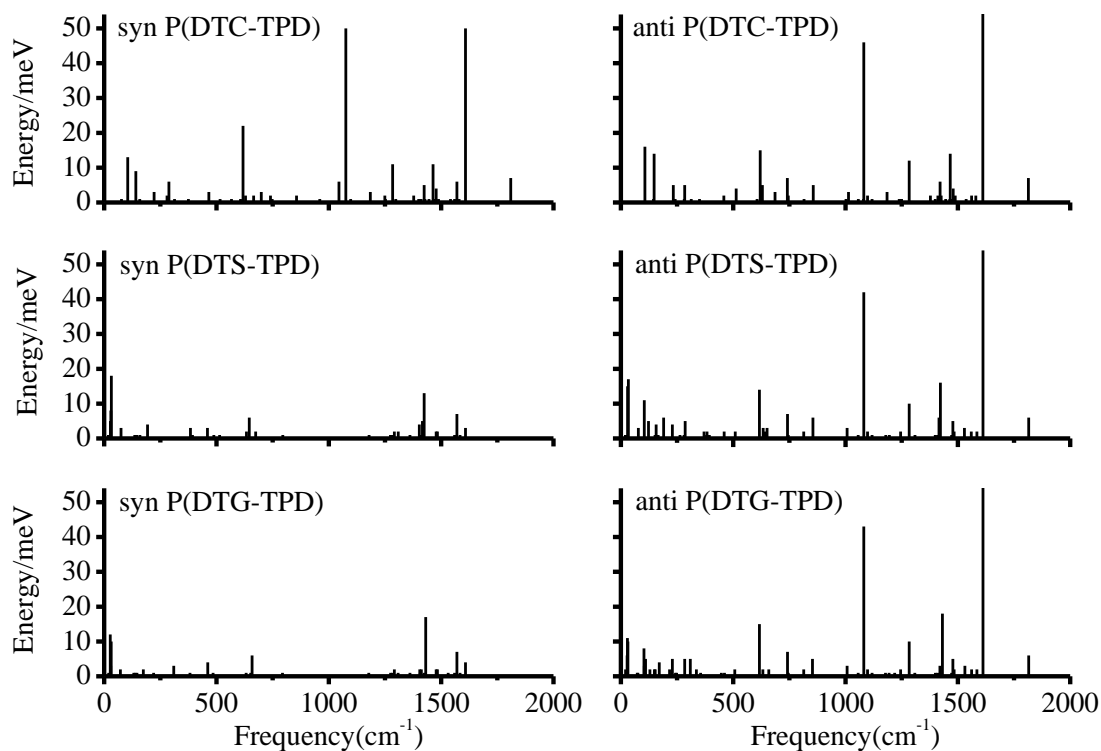


Figure S4. Contribution of the vibrational modes to the relaxation energy of the S_1 states of P(DTC-TPD), P(DTS-TPD), and P(DTG-TPD) in the syn- and anti-conformations. These calculations were performed at the B3LYP/6-31G(d) level.

Table S2. Optimal values of the range-separated parameters (in bohr⁻¹) at the ω B97XD/PCM level with the 6-31G(d) basis set.

(DTC-TPD) _{n=1}	0.023
(DTC-TPD) _{n=2}	0.015
(DTC-TPD) _{n=3}	0.012
(DTC-TPD) _{n=4}	0.010
(DTC-TPD) _{n=5}	0.009
(DTS-TPD) _{n=5}	0.009
(DTG-TPD) _{n=5}	0.009

Table S3. Energies (in eV) of the HOMO and LUMO oligomer levels at the tuned- ω B97XD/PCM level with the 6-31G(d) basis set.

	HOMO		LUMO	
	$\alpha=180^\circ$	$\alpha=0^\circ$	$\alpha=180^\circ$	$\alpha=0^\circ$
(DTC-TPD) _{n=1}	-5.27	-5.28	-1.57	-1.61
(DTC-TPD) _{n=2}	-4.98	-4.99	-2.17	-2.23
(DTC-TPD) _{n=3}	-4.89	-4.90	-2.36	-2.42
(DTC-TPD) _{n=4}	-4.84	-4.85	-2.45	-2.52
(DTC-TPD) _{n=5}	-4.82	-4.83	-2.51	-2.57
(DTS-TPD) _{n=5}	-4.91	-4.94	-2.50	-2.60
(DTG-TPD) _{n=5}	-4.89	-4.92	-2.48	-2.58

Table S4. Energies (eV) of the oligomer lowest excited singlet and triplet states at the tuned- ω B97XD/PCM with the 6-31G(d) basis set.

	S ₁		T ₁	
	$\alpha=180^\circ$	$\alpha=0^\circ$	$\alpha=180^\circ$	$\alpha=0^\circ$
(DTC-TPD) _{n=1}	2.93	2.91	1.90	1.87
(DTC-TPD) _{n=2}	2.15	2.11	1.51	1.47
(DTC-TPD) _{n=3}	1.90	1.86	1.41	1.36
(DTC-TPD) _{n=4}	1.79	1.74	1.38	1.32
(DTC-TPD) _{n=5}	1.74	1.68	1.36	1.31
Exp. P(DTC-TPD)	1.71			

Electronic Properties

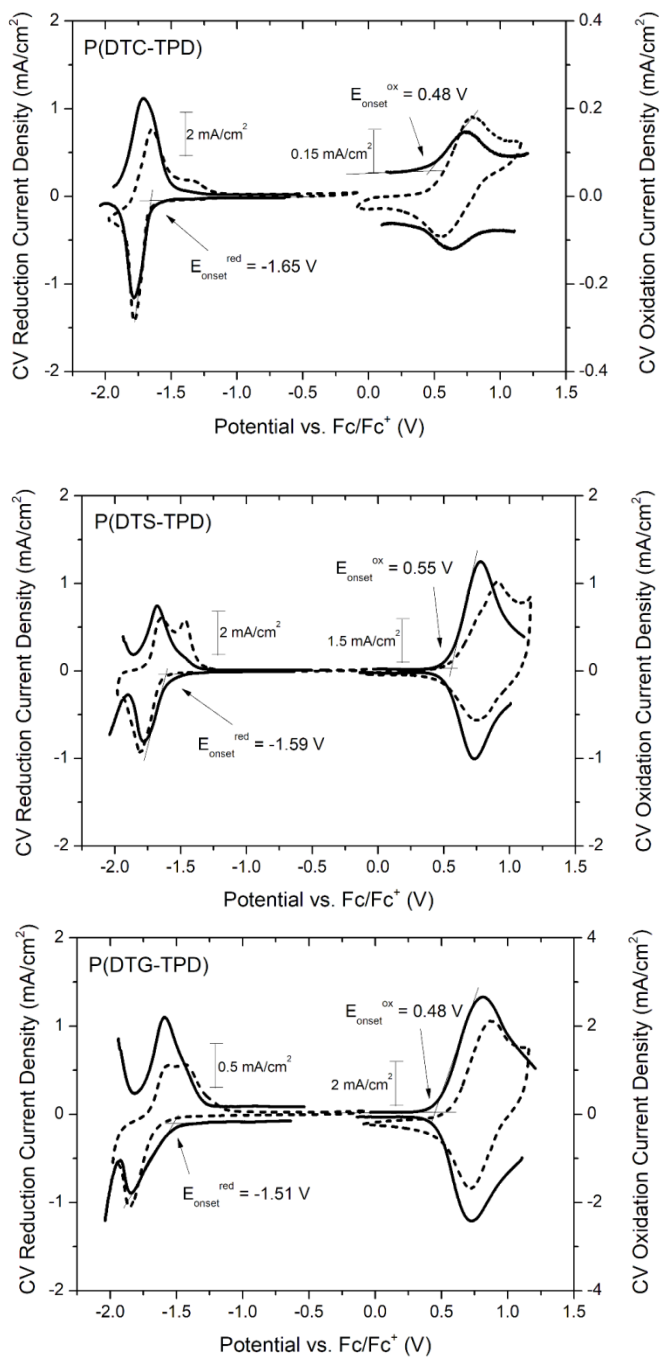


Figure S5. Cyclic voltammograms (dotted lines) and differential pulse voltammograms (solid lines) of polymers. Onsets of oxidation and reduction are calculated from DPV. Inset scale bars show DPV current densities.

Steady-state Optical Absorption Properties

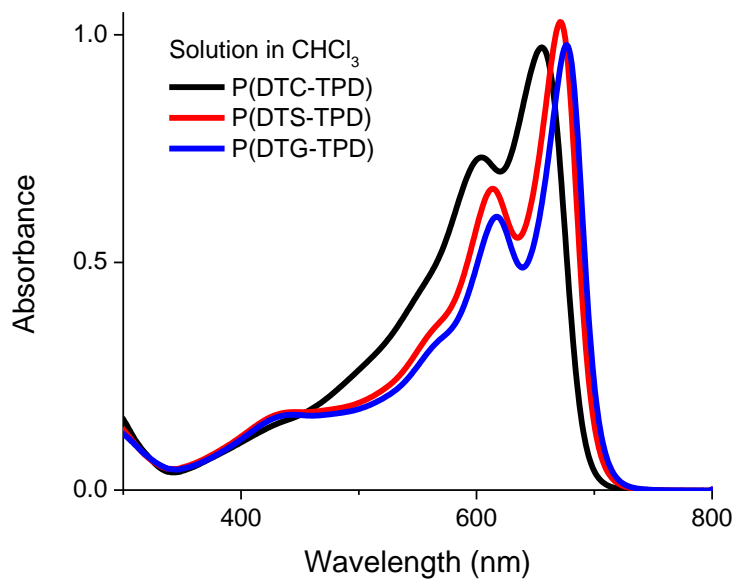


Figure S6. Solution UV-Vis absorption spectra of P(DTC-TPD), P(DTS-TPD), and P(DTG-TPD) in chloroform.

Solid State NMR Measurements and Characterizations

All solid-state NMR spectra were collected on a Bruker DSX 500 spectrometer operating at 11.7 T. A commercial Bruker 2.5 mm H/X/Y triple resonance MAS probe and 2.5 mm o.d. ZrO₂ rotors were used, employing MAS frequencies between 25.0 and 27.778 kHz. Radio-frequency nutation frequencies and ¹H chemical shifts were referenced on adamantane (1.85 ppm)²⁵ and the magic angle was set using KBr²⁶ before each measurement. The pi/2 pulse length for ¹H excitation was 2.5 μs. Double-quantum recoupling was achieved using the back-to-back (BaBa) pulse sequence,²⁷ where exact rotor-synchronization was achieved via external triggering at the beginning of the excitation and reconversion blocks. Additionally, a z-filter of one rotor period was added. Excitation periods of one and four rotor periods were chosen. To suppress t₁-noise from the mobile alkyl side-chains, a selective pre-saturation of the alkyl signals via a very low power 5 ms pulse was employed.²⁸ ¹H Background suppression was achieved via the Elimination of Artifacts in NMR Spectroscopy (EASY) protocol.²⁹ Relaxation delays were determined via the saturation-recovery method and a relaxation delay of 2 s was used for all samples. For the ¹H MAS NMR spectra 64 scans were acquired, while the 2D ¹H-¹H DQ-SQ NMR correlation spectra were acquired using either 128 (1 rotor period) or 256 (4 rotor periods) scans for a total of 96 rotor-synchronized t₁-increments. Phase-sensitive 2D NMR data were obtained using the STATES-TPPI method.³⁰ All 2D NMR spectra were zero-filled to 4096 and 256 points in the direct and indirect dimension, respectively, and apodized with a Gaussian window function (25 Hz) before 2D Fourier transformation. Contour levels are shown from 2.5% to 100% of the maximum intensity. Further data analysis, processing and plotting was done with the Bruker Topspin software and dmFit package.³¹

To determine the relative intensities of the two conformations, we have performed a line-shape deconvolution of the aromatic region using the dmFit software as summarized in Figure S7. The spectral resolution was enhanced using a TRAF window function (250 Hz).³¹

For DFT calculation of NMR parameters geometry optimization with TURBOMOLE (version 6.5)^{32,33} was performed. Using the meta-GGA functional TPSS³⁴ in combination with an Ahlrichs' def2-TZVP basis set³⁵ gained from the EMSL database^{36,37} proved to be sufficient. Additionally D3 dispersion correction^{38,39} and the RI-Ansatz were applied. Convergence criteria were set to 10⁻⁷ E_H for SCF and 5·10⁻⁷ E_H for the geometry optimization respectively. The NMR shift calculations were performed using the same set of parameters and the B3LYP^{40,41} functional to enhance the accuracy.

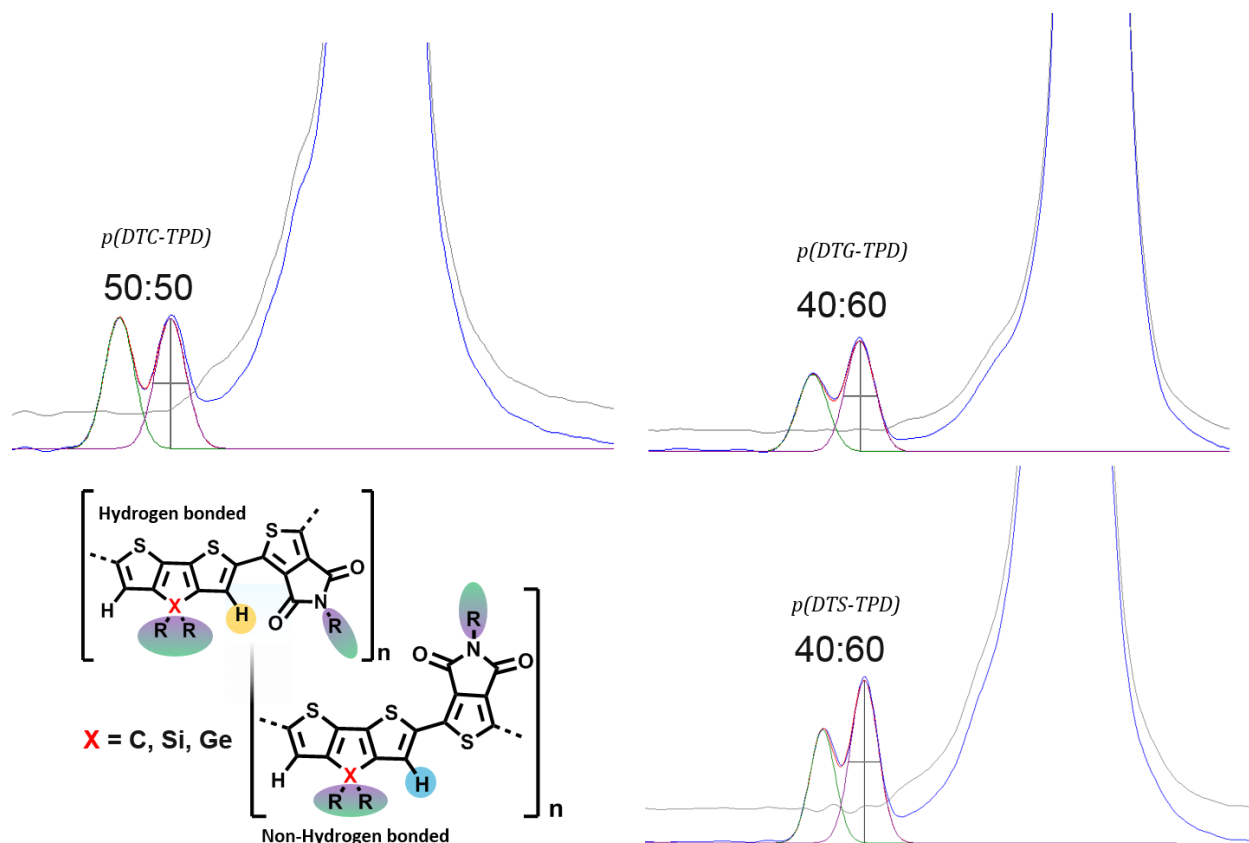


Figure S7. ^1H MAS NMR spectra of P(DTC-TPD), P(DTS-TPD), and P(DTG-TPD) showing the spectral deconvolution.

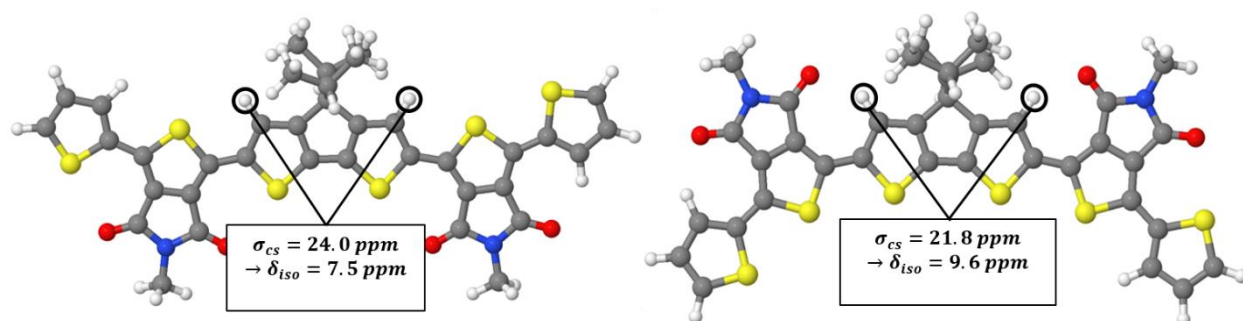


Figure S8. Calculated isotropic ^1H chemical shielding and shift values (σ_{CS} and δ_{iso}) for the aromatic protons of the DTC group, assuming that in one case they (right) have hydrogen-carbonyl intra-molecular interaction and another case (left) they have no hydrogen-carbonyl intra-molecular interaction due to the anti-conformation of the TPD group. The ^1H chemical shielding values were converted into chemical shift values via calculations for a number of reference compounds with known experimental ^1H chemical shifts.

OPV Device Fabrication and Characterization

Methods

Devices were fabricated in the conventional architecture (Al/LiF/Polymer:PC₇₁BM/PEDOT:PSS/ITO). Patterned ITO substrates supplied by Tinwell Technology (tinwell@incnets.com, project TI1678D) were cleaned by sonication for 15 minutes each in 0.1% sodium dodecyl sulfate solution, ultrapure water (Millipore system, resistivity 18.2 MΩ.cm), acetone, and isopropyl alcohol. The substrates were exposed to UV-ozone for two 10-minute treatments. PEDOT:PSS (Clevios™ P VP AI 4083) was purchased from Heraeus Deutschland GmbH & Co. KG. and was spin-coated in air onto the ITO substrate at 5,000 RPM for one minute (45 nm) and annealed at 140 °C for 20 min. Polymer:PC₇₁BM blends (1:1.5 ratio, 20 mg/mL in chlorobenzene) were dissolved and stirred for 16 hours at 70 °C under in a argon-filled glovebox. Processing additive, 5% (v/v) 1,8-diiodooctane (DIO), was added to the solution before deposition. The active layer was spin coated on top of the PEDOT:PSS layer. All substrates were then transferred into a thermal evaporator in which LiF (1 nm) and Al (100 nm) were deposited on top of the active layer at 10⁻⁶ torr through a metal mask

Current density–voltage (J–V) characteristics were measured using a Keithley 4200 semiconductor parameter analyzer system with a Newport Thermal Oriel 94021 1000 W solar simulator, using the AM1.5 G solar spectrum at 100 mW/cm² incident power. Hole-only devices with a structure ITO/molybdenum oxide (MoOx)(8 nm)/active layer(90 nm)/MoOx(8 nm)/silver (Ag)(100 nm) were used for hole mobility measurements, and electron-only devices with a structure of ITO/zinc oxide (ZnO)(40 nm)/active layer(90 nm)/LiF(1 nm)/Al(100 nm) were used for electron mobilities measurements. External quantum efficiency (EQE) measurements were conducted using an in-house setup consisting of a xenon dc arc lamp, an ORIEL 74125 monochromator, a Keithley 428 current amplifier, an SR 540 chopper system, and an SR830 DSP lock-in amplifier from SRS.

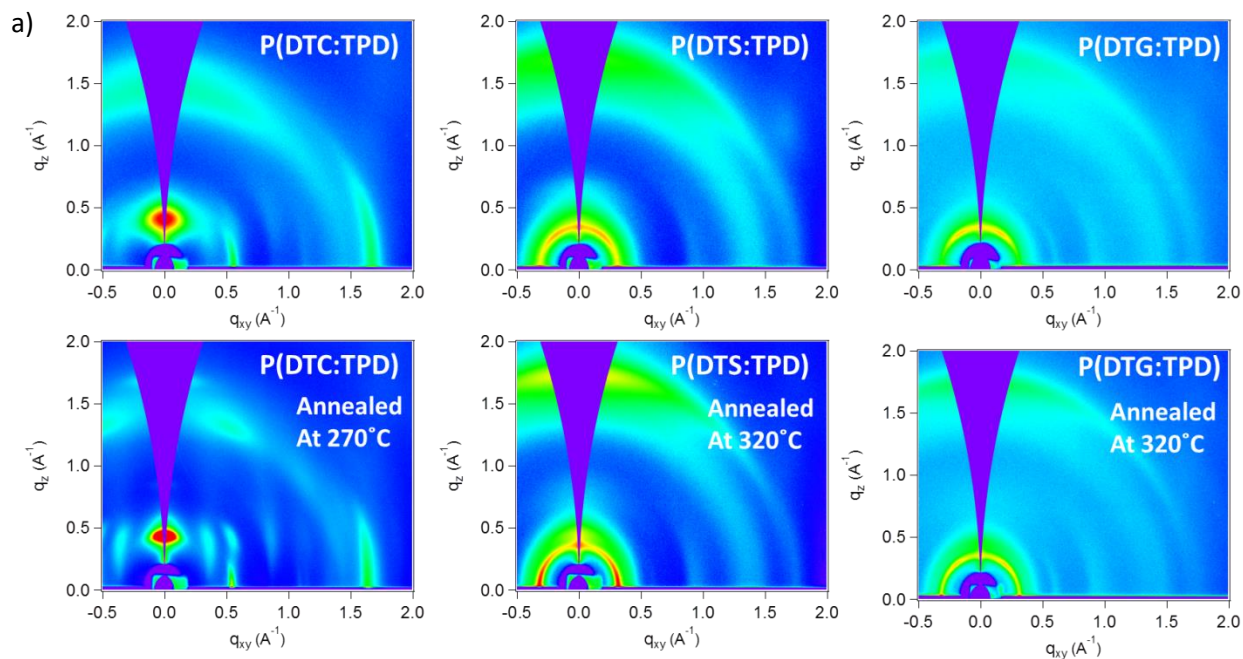
Device capacitance was measured using a HIOKI 3523-50 LRC meter. Film thicknesses were measured using a Bruker's Dektak stylus profiler. To eliminate the parasitic effect, devices were calibrated at the short and open circuit condition. The capacitance of the device was measured at 100 kHz with a small 20 mV AC modulation. For the measurement of electroabsorption spectroscopy, the samples were probed using monochromatic light directed into the sample through ITO with an incident angle of 45°. The beam was reflected by the back Al electrode and captured by calibrated silicon and germanium photodetectors. The internal electric field of the sample was modulated using a DC bias superimposed with a small AC voltage at a modulation frequency of 1000 Hz. A current amplifier and a lock-in amplifier were connected to the photodetector to increase the signal-to-noise ratio.

Table S5. Dielectric constants of polymers and transport properties of polymer:fullerene blends.

Device	Pristine Polymer	Polymer: Fullerene	Hole Mobility cm^2/Vs	Electron Mobility cm^2/Vs
	ϵ_r	ϵ_r		
P(DTC-TPD)	2.8 ± 0.2	4.7 ± 0.3	$5.2 \cdot 10^{-4} \pm 1.7 \cdot 10^{-5}$	$2.9 \cdot 10^{-3} \pm 2.8 \cdot 10^{-4}$
P(DTS-TPD)	2.2 ± 0.1	5.2 ± 0.2	$1.4 \cdot 10^{-3} \pm 3.3 \cdot 10^{-5}$	$2.8 \cdot 10^{-3} \pm 5.2 \cdot 10^{-4}$
P(DTG-TPD)	2.4 ± 0.1	5.5 ± 0.2	$4.3 \cdot 10^{-4} \pm 3.5 \cdot 10^{-5}$	$2.4 \cdot 10^{-3} \pm 1.8 \cdot 10^{-4}$

X-Ray Diffraction Measurement with Thermal Annealing

GIWAXS measurements were performed on beamline 11-3 at the Stanford Synchrotron Radiation Lightsource. Thin films were deposited onto silicon wafers (100) with the same conditions as in device fabrications. The samples were placed in a helium-purged chamber. The photon energy was 12.7 keV. The incidence angle was set to 0.20° , slightly above the critical angle for these materials. Diffraction was recorded using a Rayonix MX225 X-ray detector, and processed using the Nika software package for Wavemetrics Igor Pro,⁴² in combination with custom written Igor scripts to map the detector data to reciprocal space using equations published by Stribeck and Noechel.⁴³ The images were calibrated using a lanthanum hexaboride (LaB_6) standard. Each substrate was loaded into a helium-purged chamber to reduce air scattering and beam damage to the samples. X-ray irradiation durations varied from one to five minutes depending on the desirable signal intensity. Images were analyzed using the WxDiff software. The signals were analyzed according to the modified Bragg's law, $q = 2\pi/\lambda$.

**Figure S9.** GIWAXS patterns for pristine polymer thin-films as-cast (top) and post temperature annealing (bottom).

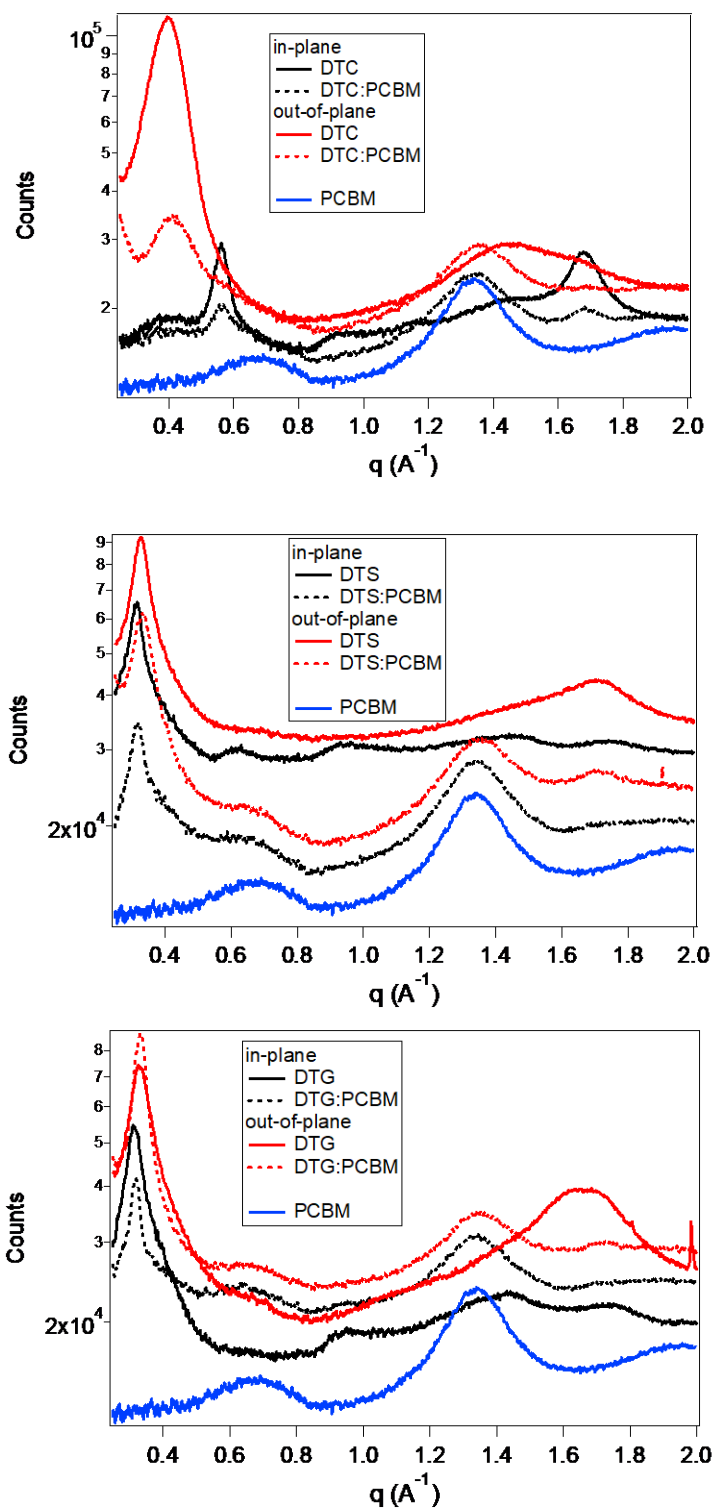


Figure S10. Integration of the GIWAXS patterns for the polymers. The out-of-plane (OOP) data is integrated cakeslice at 0-20 degrees and the in-plane (IP) data is cakeslice at 70-90 degrees (the horizon was removed).

Thermal Transition of Polymers

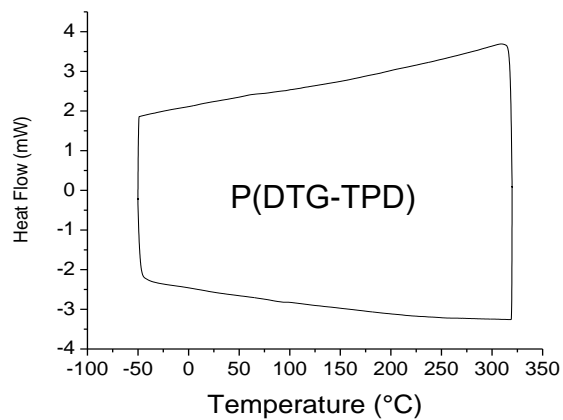
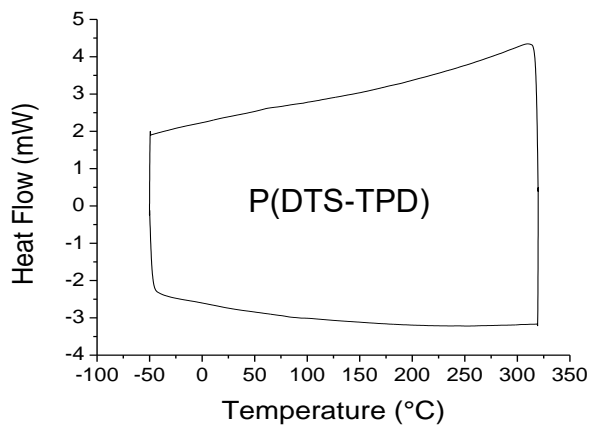
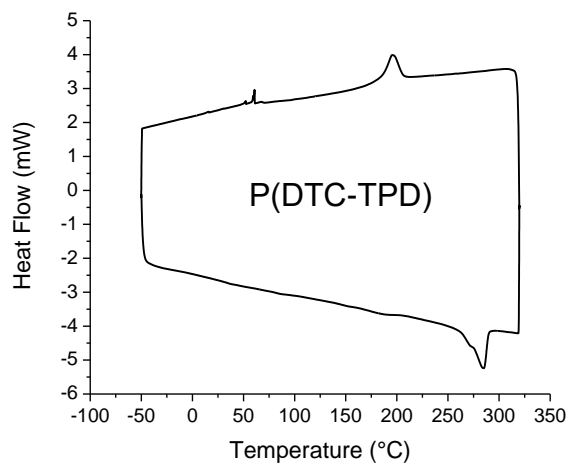


Figure S11. Differential scanning calorimetry traces of polymers at a rate of 10 °C/min.

Topographical Characteristic of Polymer:PCBM Thin Films

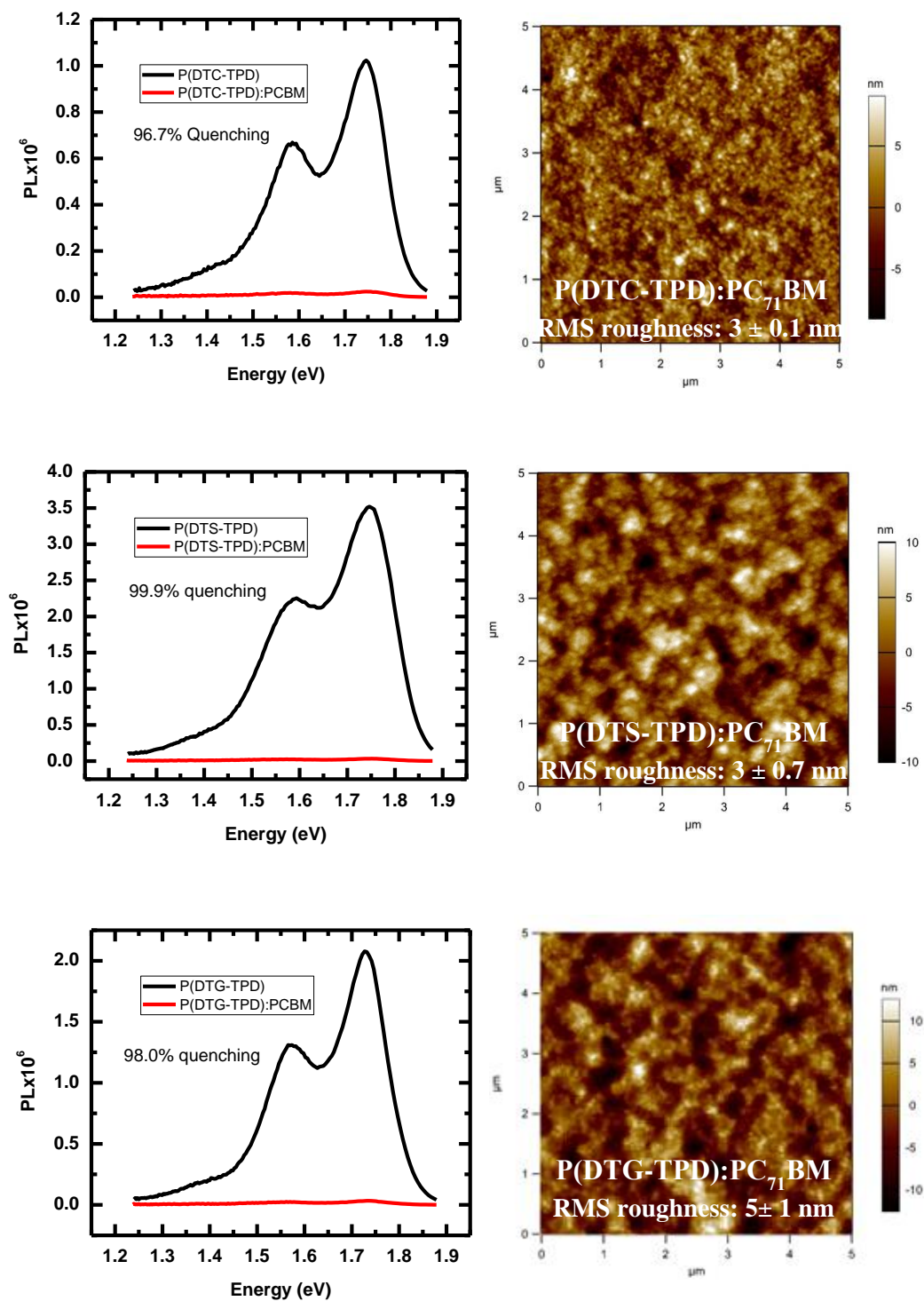


Figure S12. PL spectra of neat polymer and polymer:PC₇₁BM films. AFM height images of polymer:PCBM (1:1.5) blends.

Transient Absorption Properties

Transient absorption data were collected using transient absorption spectroscopy setup. This setup consists of the spectrometer (Ultrafast Helios system) and amplified Ti:Sapphire Laser. The output of amplified Ti:Sapphire Laser provides 800 nm fundamental pulses at 1kHz repetition rate which were splitted into two optical beams to generate pump and probe pulses. One fundamental beam was used to generate pump beam using an optical parametric amplifier (OPA) system (Coherent Opera Solo). A white light/NIR probe was generated by focusing the another fundamental beam into a flint glass. Pump and probe beams were focused on a sample and probe light was collected by a charge-coupled device CCD device. The spectral detection region is 0.8 eV to 1.6 eV. The thin film samples were encapsulated using UV curable glue before measurement. The instrument response function (IRF) was ~ 100 fs FWHM. The samples were excited with the excitation energy 1.91 eV (650 nm) and the fractional change in transmission was detected in the probe range 0.8-1.6 eV at several time delays.

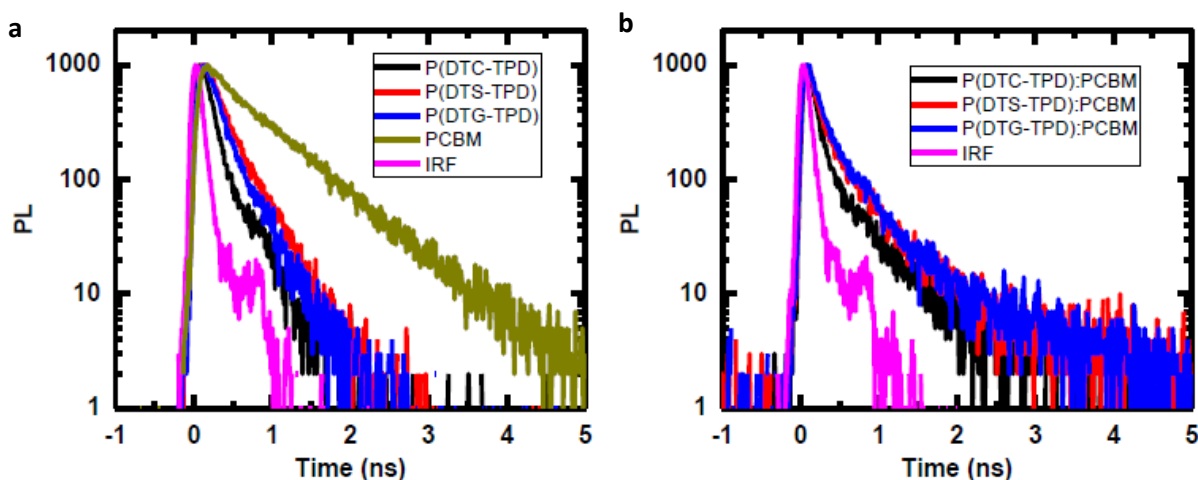


Figure S13. PL dynamics for (a) Neat donor and acceptor films (b) Blended films. Neat donor films are P(DTC-TPD), P(DTS-TPD), and P(DTG-TPD) and acceptor film is PC₇₁BM. Blend films are P(DTC-TPD):PC₇₁BM, P(DTS-TPD):PC₇₁BM and P(DTG-TPD):PC₇₁BM. Instrument response function (IRF) signals are plot as comparisons.

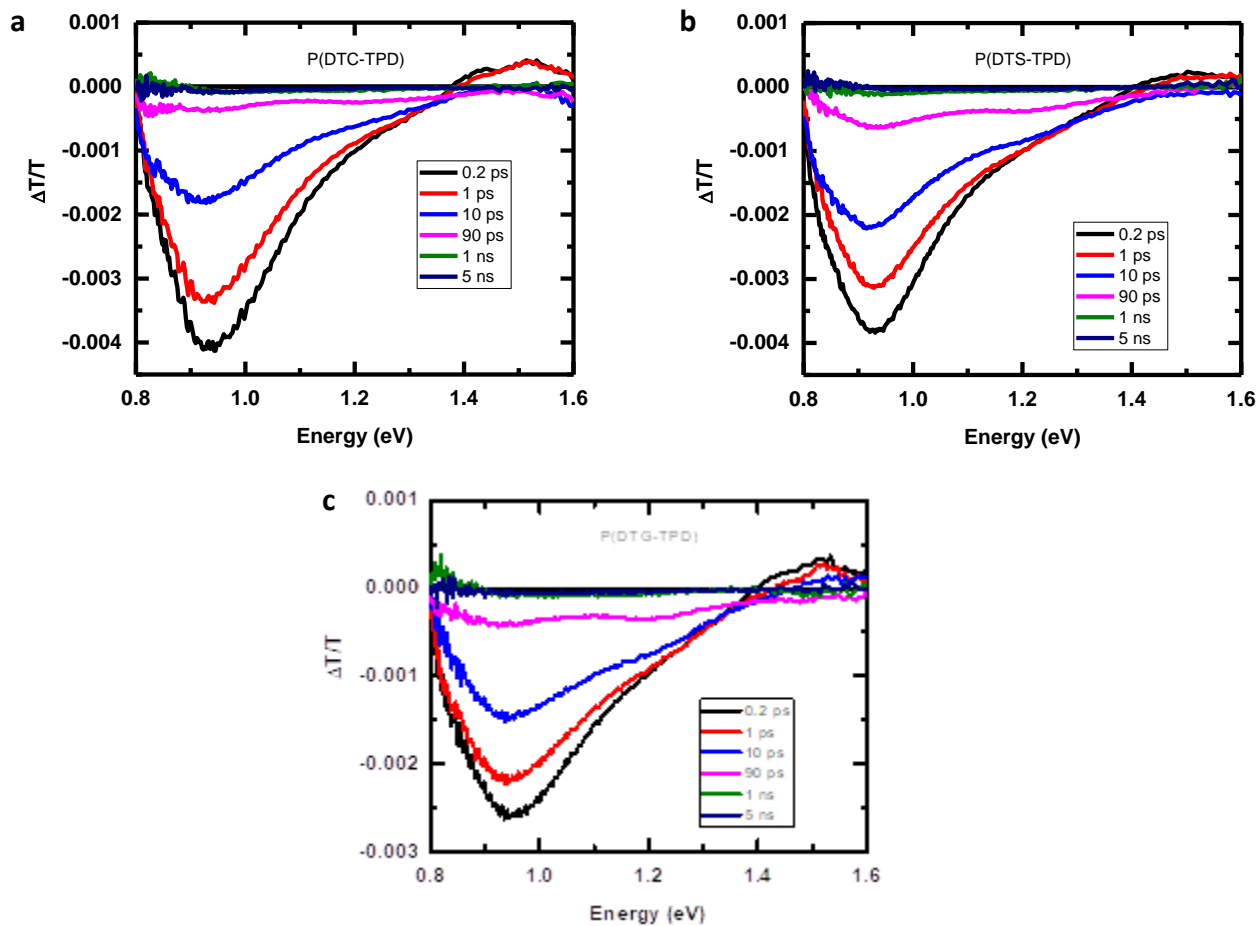


Figure S14. Transient absorption spectra of (a) P(DTC-TPD), (b) P(DTS-TPD) and (c) P(DTG-TPD) films.

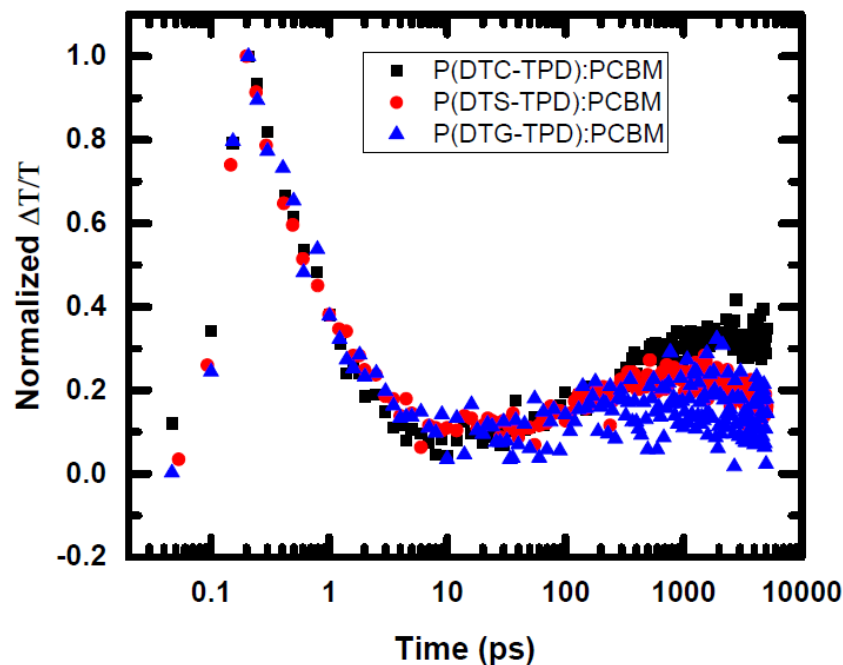


Figure S15. Singlet exciton PIA dynamics given by the early dynamics of 0.95 eV peak for P(DTC-TPD):PC₇₁BM, P(DTS-TPD):PC₇₁BM and P(DTG-TPD):PC₇₁BM films.

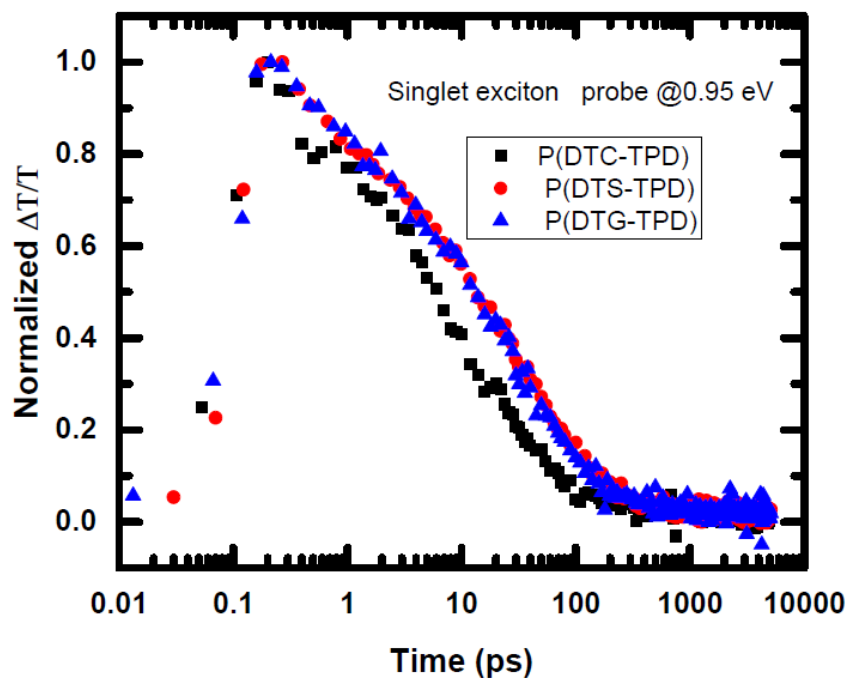


Figure S16. Singlet exciton PIA dynamics P(DTC-TPD), P(DTS-TPD) and P(DTG-TPD).

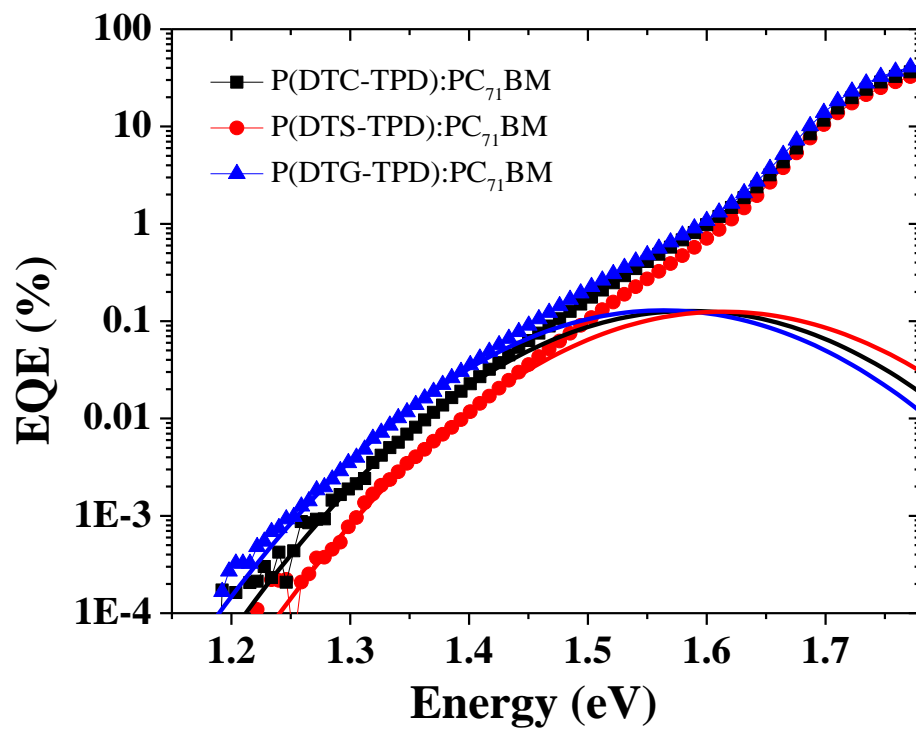


Figure S17. Sub-bandgap EQE plots of polymer:fullerene blends. The fitting of the shoulder-like features were used to estimate the charge transfer energies, ~ 1.40 eV.

References

- (1) Cardona, C. M.; Li, W.; Kaifer, A. E.; Stockdale, D.; Bazan, G. C. Electrochemical Considerations for Determining Absolute Frontier Orbital Energy Levels of Conjugated Polymers for Solar Cell Applications. *Adv. Mater.* **2011**, *23*, 2367–2371.
- (2) Rasmussen, S. C. The Nomenclature of Fused-Ring Arenes and Heterocycles: A Guide to an Increasingly Important Dialect of Organic Chemistry. *ChemTexts* **2016**, *2*, 16.
- (3) Zhu, Z.; Waller, D.; Gaudiana, R.; Morana, M.; Mühlbacher, D.; Scharber, M.; Brabec, C. Panchromatic Conjugated Polymers Containing Alternating Donor/Acceptor Units for Photovoltaic Applications. *Macromolecules* **2007**, *40*, 1981–1986.
- (4) Amb, C. M.; Chen, S.; Graham, K. R.; Subbiah, J.; Small, C. E.; So, F.; Reynolds, J. R. Dithienogermole As a Fused Electron Donor in Bulk Heterojunction Solar Cells. *J. Am. Chem. Soc.* **2011**, *133*, 10062–10065.
- (5) Hou, J.; Chen, H.-Y.; Zhang, S.; Li, G.; Yang, Y. Synthesis, Characterization, and Photovoltaic Properties of a Low Band Gap Polymer Based on Silole-Containing Polythiophenes and 2,1,3-Benzothiadiazole. *J. Am. Chem. Soc.* **2008**, *130*, 16144–16145.
- (6) Nielsen, C. B.; Bjørnholm, T. New Regiosymmetrical Dioxopyrrolo- and Dihydropyrrolo-Functionalized Polythiophenes. *Org. Lett.* **2004**, *6*, 3381–3384.
- (7) Berrouard, P.; Pron, A.; Veilleux, J.; Leclerc, M. Low-Cost Synthesis and Physical Characterization of Thieno[3,4-C]pyrrole-4,6-Dione-Based Polymers. *J. Org. Chem.* **2012**, *77*, 8167–8173.
- (8) Zhang, Y.; Zou, J.; Yip, H.-L.; Sun, Y.; Davies, J. A.; Chen, K.-S.; Acton, O.; Jen, A. K.-Y. Conjugated Polymers Based on C, Si and N-Bridged Dithiophene and Thienopyrroledione Units: Synthesis, Field-Effect Transistors and Bulk Heterojunction Polymer Solar Cells. *J. Mater. Chem.* **2011**, *21*, 3895.
- (9) Hong, Y. R.; Ng, J. Y.; Wong, H. K.; Moh, L. C. H.; Yip, Y. J.; Chen, Z. K.; Norsten, T. B. Synthesis and Characterization of a Series of Low-Bandgap Copolymers Based on cyclopenta[2,1-b:3,4-B']dithiophene and Thienopyrroledione for Photovoltaic Applications. *Sol. Energ. Mat. Sol. Cells* **2012**, *102*, 58–65.
- (10) Zhao, X.; Tang, H.; Yang, D.; Li, H.; Xu, W.; Yin, L.; Yang, X. Effect of Molecular Weight and Processing Additive on the Performance of Low Bandgap Polymer Solar Cells. *Chin. J. Chem.* **2012**, *30*, 2052–2058.
- (11) Cai, W.; Liu, P.; Jin, Y.; Xue, Q.; Liu, F.; Russell, T. P.; Huang, F.; Yip, H.-L.; Cao, Y. Morphology Evolution in High-Performance Polymer Solar Cells Processed from Nonhalogenated Solvent. *Adv. Sci.* **2015**, *2*, 1500095.
- (12) Aïch, B. R.; Beaupré, S.; Leclerc, M.; Tao, Y. Highly Efficient thieno[3,4-C]pyrrole-4,6-Dione-Based Solar Cells Processed from Non-Chlorinated Solvent. *Org. Electron.* **2014**, *15*, 543–548.

- (13) Guo, X.; Zhou, N.; Lou, S. J.; Hennek, J. W.; Ponce Ortiz, R.; Butler, M. R.; Boudreault, P. L. T.; Strzalka, J.; Morin, P. O.; Leclerc, M.; López Navarrete, J. T.; Ratner, M. A.; Chen, L. X.; Chang, R. P. H.; Facchetti, A.; Marks, T. J. Bithiopheneimide-Dithienosilole/dithienogermole Copolymers for Efficient Solar Cells: Information from Structure-Property-Device Performance Correlations and Comparison to thieno[3,4-c]Pyrrole-4,6-Dione Analogues. *J. Am. Chem. Soc.* **2012**, *134*, 18427–18439.
- (14) Gendron, D.; Morin, P.-O.; Berrouard, P.; Allard, N.; Aïch, B. R.; Garon, C. N.; Tao, Y.; Leclerc, M. Synthesis and Photovoltaic Properties of Poly (Dithieno Germole) Derivatives. *Macromolecules* **2011**, *44*, 7188–7193.
- (15) Constantinou, I.; Lai, T.-H.; Zhao, D.; Klump, E. D.; Deininger, J. J.; Lo, C. K.; Reynolds, J. R.; So, F. High Efficiency Air-Processed Dithienogermole-Based Polymer Solar Cells. *ACS Appl. Mater. Interfaces* **2015**, *7*, 4826–4832.
- (16) Small, C. E.; Chen, S.; Subbiah, J.; Amb, C. M.; Tsang, S.-W.; Lai, T.-H.; Reynolds, J. R.; So, F. High-Efficiency Inverted Dithienogermole–thienopyrrolodione-Based Polymer Solar Cells. *Nat. Photon.* **2012**, *6*, 115–120.
- (17) Chai, J.-D.; Head-Gordon, M.; Laming, G. J.; Shao, Y.; Head-Gordon, M.; Brown, S. T.; Gilbert, A. T. B.; Slipchenko, L. V.; Levchenko, S. V.; O’Neill, D. P.; Jr., R. A. D.; Lochan, R. C.; Wang, T.; Beran, G. J. O.; Besley, N. A.; Herbert, J. M.; Lin, C. Y.; Voorhis, T. Van; Chien, S. H.; Sodt, A.; Steele, R. P.; Rassolov, V. A.; Maslen, P. E.; Korambath, P. P.; Adamson, R. D.; Austin, B.; Baker, J.; Byrd, E. F. C.; Dachsel, H.; Doerksen, R. J.; Dreuw, A.; Dunietz, B. D.; Dutoi, A. D.; Furlani, T. R.; Gwaltney, S. R.; Heyden, A.; Hirata, S.; Hsu, C.-P.; Kedziora, G.; Khalliulin, R. Z.; Klunzinger, P.; Lee, A. M.; Lee, M. S.; Liang, W.; Lotan, I.; Nair, N.; Peters, B.; Proynov, E. I.; Pieniazek, P. A.; Rhee, Y. M.; Ritchie, J.; Rosta, E.; Sherrill, C. D.; Simmonett, A. C.; Subotnik, J. E.; III, H. L. W.; Zhang, W.; Bell, A. T.; Chakraborty, A. K.; Chipman, D. M.; Keil, F. J.; Warshel, A.; Hehre, W. J.; III, H. F. S.; Kong, J.; Krylov, A. I.; Gill, P. M. W.; Head-Gordon, M. Long-Range Corrected Hybrid Density Functionals with Damped Atom–atom Dispersion Corrections. *Phys. Chem. Chem. Phys.* **2008**, *10*, 6615.
- (18) Stein, T.; Kronik, L.; Baer, R. Prediction of Charge-Transfer Excitations in Coumarin-Based Dyes Using a Range-Separated Functional Tuned from First Principles. *J. Chem. Phys.* **2009**, *131*, 244119.
- (19) Mennucci, B.; Tomasi, J. Continuum Solvation Models: A New Approach to the Problem of Solute’s Charge Distribution and Cavity Boundaries. *J. Chem. Phys.* **1997**, *106*, 5151.
- (20) Zheng, Z.; Brédas, J.-L.; Coropceanu, V. Description of the Charge Transfer States at the Pentacene/C 60 Interface: Combining Range-Separated Hybrid Functionals with the Polarizable Continuum Model. *J. Phys. Chem. Lett.* **2016**, *7*, 2616–2621.
- (21) Malagoli, M.; Coropceanu, V.; da Silva Filho, D. A.; Brédas, J. L. A Multimode Analysis of the Gas-Phase Photoelectron Spectra in Oligoacenes. *J. Chem. Phys.* **2004**, *120*, 7490–7496.
- (22) Gaussian 09; Frisch, M. J.; Trucks, G. W.; Schlegel, H. B.; Scuseria, G. E.; Robb, M. A.;

- Cheeseman, J. R.; Scalmani, G.; Barone, V.; Petersson, G. A.; Nakatsuji, H.; Li, X.; Caricato, M.; Marenich, A.; Bloino, J.; Janesko, B. G.; Gomperts, R.; Mennucci, B.; Hratchian, H. P.; Ortiz, J. V.; Izmaylov, A. F.; Sonnenberg, J. L.; Williams-Young, D.; Ding, F.; Lipparini, F.; Egidi, F.; Goings, J.; Peng, B.; Petrone, A.; Henderson, T.; Ranasinghe, D.; Zakrzewski, V. G.; Gao, J.; Rega, N.; Zheng, G.; Liang, W.; Hada, M.; Ehara, M.; Toyota, K.; Fukuda, R.; Hasegawa, J.; Ishida, M.; Nakajima, T.; Honda, Y.; Kitao, O.; Nakai, H.; Vreven, T.; Throssell, K.; Montgomery, J. A. J.; Peralta, J. E.; Ogliaro, F.; Bearpark, M.; Heyd, J. J.; Brothers, E.; Kudin, K. N.; Staroverov, V. N.; Keith, T.; Kobayashi, R.; Normand, J.; Raghavachari, K.; Rendell, A.; Burant, J. C.; Iyengar, S. S.; Tomasi, J.; Cossi, M.; Millam, J. M.; Klene, M.; Adamo, C.; Cammi, R.; Ochterski, J. W.; Martin, R. L.; Morokuma, K.; Farkas, O.; Foresman, J. B.; Fox, D. J. Gaussian 09, Revision A.02. Gaussian, Inc.: Wallingford CT 2009.
- (23) Shao, Y.; Molnar, L. F.; Jung, Y.; Kussmann, J.; Ochsenfeld, C.; Brown, S. T.; Gilbert, A. T. B.; Slipchenko, L. V.; Levchenko, S. V.; O'Neill, D. P.; DiStasio Jr, R. A.; Lochan, R. C.; Wang, T.; Beran, G. J. O.; Besley, N. A.; Herbert, J. M.; Yeh Lin, C.; Van Voorhis, T.; Hung Chien, S.; Sodt, A.; Steele, R. P.; Rassolov, V. A.; Maslen, P. E.; Korambath, P. P.; Adamson, R. D.; Austin, B.; Baker, J.; Byrd, E. F. C.; Dachsel, H.; Doerksen, R. J.; Dreuw, A.; Dunietz, B. D.; Dutoi, A. D.; Furlani, T. R.; Gwaltney, S. R.; Heyden, A.; Hirata, S.; Hsu, C.-P.; Kedziora, G.; Khalliulin, R. Z.; Klunzinger, P.; Lee, A. M.; Lee, M. S.; Liang, W.; Lotan, I.; Nair, N.; Peters, B.; Proynov, E. I.; Pieniazek, P. A.; Min Rhee, Y.; Ritchie, J.; Rosta, E.; David Sherrill, C.; Simmonett, A. C.; Subotnik, J. E.; Lee Woodcock III, H.; Zhang, W.; Bell, A. T.; Chakraborty, A. K.; Chipman, D. M.; Keil, F. J.; Warshel, A.; Hehre, W. J.; Schaefer III, H. F.; Kong, J.; Krylov, A. I.; Gill, P. M. W.; Head-Gordon, M. Advances in Methods and Algorithms in a Modern Quantum Chemistry Program Package. *Phys. Chem. Chem. Phys.* **2006**, *8*, 3172–3191.
- (24) Krylov, A. I.; Gill, P. M. W. Q-Chem: An Engine for Innovation. *Wiley. Interdiscip. Rev. Comput. Mol. Sci.* **2013**, *3*, 317–326.
- (25) Hayashi, S.; Hayamizu, K. Chemical Shift Standards in High-Resolution Solid-State NMR (1) ¹³C, ²⁹Si, and ¹H Nuclei. *Bull. Chem. Soc. Jpn.* **1991**, *64*, 685–687.
- (26) Frye, J. S.; Maciel, G. E. Setting the Magic Angle Using a Quadrupolar Nuclide. *J. Magn. Reson.* **1982**, *48*, 125–131.
- (27) Brown, S. P.; Zhu, X. X.; Saalwächter, K.; Spiess, H. W. An Investigation of the Hydrogen-Bonding Structure in Bilirubin by ¹H Double-Quantum Magic-Angle Spinning Solid-State NMR Spectroscopy. *J. Am. Chem. Soc.* **2001**, *123*, 4275–4285.
- (28) Robertson, A. J.; Pandey, M. K.; Marsh, A.; Nishiyama, Y.; Brown, S. P. The Use of a Selective Saturation Pulse to Suppress t1 Noise in Two-Dimensional ¹H Fast Magic Angle Spinning Solid-State NMR Spectroscopy. *J. Magn. Reson.* **2015**, *260*, 89–97.
- (29) Jaeger, C.; Hemmann, F. EASY: A Simple Tool for Simultaneously Removing Background, Deadtime and Acoustic Ringing in Quantitative NMR spectroscopy—Part I: Basic Principle and Applications. *Solid State Nucl. Magn. Reson.* **2014**, *57*, 22–28.
- (30) Marion, D.; Ikura, M.; Tschudin, R.; Bax, A. Rapid Recording of 2D NMR Spectra

- without Phase Cycling. Application to the Study of Hydrogen Exchange in Proteins. *J. Magn. Reson.* **1989**, *85*, 393–399.
- (31) Massiot, D.; Fayon, F.; Capron, M.; King, I.; Le Calvé, S.; Alonso, B.; Durand, J.-O.; Bujoli, B.; Gan, Z.; Hoatson, G. Modelling One- and Two-Dimensional Solid-State NMR Spectra. *Magn. Reson. Chem.* **2002**, *40*, 70–76.
- (32) TURBOMOLE V6.5 2013, a development of University of Karlsruhe and Forschungszentrum Karlsruhe GmbH, 1989-2007, TURBOMOLE GmbH, since 2007 <http://www.turbolome.com>.
- (33) Ahlrichs, R.; Bär, M.; Häser, M.; Horn, H.; Kölmel, C. Electronic Structure Calculations on Workstation Computers: The Program System Turbomole. *Chem. Phys. Lett.* **1989**, *162*, 165–169.
- (34) Tao, J.; Perdew, J. P.; Staroverov, V. N.; Scuseria, G. E. Climbing the Density Functional Ladder: Nonempirical Meta-Generalized Gradient Approximation Designed for Molecules and Solids. *Phys. Rev. Lett.* **2003**, *91*, 146401.
- (35) Weigend, F.; Ahlrichs, R. Balanced Basis Sets of Split Valence, Triple Zeta Valence and Quadruple Zeta Valence Quality for H to Rn: Design and Assessment of Accuracy. *Phys. Chem. Chem. Phys.* **2005**, *7*, 3297–3305.
- (36) Feller, D. The Role of Databases in Support of Computational Chemistry Calculations. *J. Comput. Chem.* **1996**, *17*, 1571–1586.
- (37) Schuchardt, K. L.; Didier, B. T.; Elsethagen, T.; Sun, L.; Gurumoorthi, V.; Chase, J.; Li, J.; Windus, T. L. Basis Set Exchange: A Community Database for Computational Sciences. *J. Chem. Inf. Model.* **2007**, *47*, 1045–1052.
- (38) Grimme, S.; Antony, J.; Ehrlich, S.; Krieg, H. A Consistent and Accurate Ab Initio Parametrization of Density Functional Dispersion Correction (DFT-D) for the 94 Elements H-Pu. *J. Chem. Phys.* **2010**, *132*, 154104.
- (39) Grimme, S.; Ehrlich, S.; Goerigk, L. Effect of the Damping Function in Dispersion Corrected Density Functional Theory. *J. Comput. Chem.* **2011**, *32*, 1456–1465.
- (40) Becke, A. D. Density-functional Thermochemistry. III. The Role of Exact Exchange. *J. Chem. Phys.* **1993**, *98*, 5648–5652.
- (41) Stephens, P. J.; Devlin, F. J.; Chabalowski, C. F.; Frisch, M. J. Ab Initio Calculation of Vibrational Absorption and Circular Dichroism Spectra Using Density Functional Force Fields. *J. Phys. Chem.* **1994**, *98*, 11623–11627.
- (42) Ilavsky, J. Nika: Software for Two-Dimensional Data Reduction. *J. Appl. Crystallogr.* **2012**, *45*, 324–328.
- (43) Stribeck, N.; Nöchel, U. Direct Mapping of Fiber Diffraction Patterns into Reciprocal Space. *J. Appl. Crystallogr.* **2009**, *42*, 295–301.